GEOPHYSICS, VOL. 81, NO. 6 (NOVEMBER-DECEMBER 2016); P. T285–T293, 5 FIGS., 2 TABLES.
10.1190/GEO2016-0067.1

Laboratory evidence for Krauklis-wave resonance in fractures and implications for seismic coda wave analysis

Pei-Ju Rita Shih[1] and Marcel Frehner[1]

ABSTRACT

Krauklis waves are of major interest because they can lead to resonance effects in fluid-filled fractures. This resonance is marked by seismic signals with a dominant signature frequency, which may reveal fracture-related rock properties. In our laboratory study, we used homogeneous Plexiglas samples containing a single well-defined (i.e., manufactured) fracture. We recorded the signals obtained from propagating ultrasonic P- and S-waves (source frequency: 0.6, 1, and 2.25 MHz) along a sample without a fracture and samples with a fracture with different inclination angles of 30°, 45°, and 60° with respect to the short axis. The experimental results obtained from an incident S-wave confirmed that the presence of the fracture led to resonance effects at frequencies lower than the dominant source frequency, which slowly decayed over time in the recorded seismic coda after the first arrival. The resonance frequency was independent of the fracture orientation and the source frequency. We have interpreted this narrow-banded coda signal as a resonance in the fracture, and the frequency at which this occurred was an intrinsic property of the fracture size and elastic properties. To verify our laboratory results, we used an analytical solution, which provided a relationship between the fracture width, fracture length, resonance frequency, and temporal quality factor (i.e., exponential decay over time). The temporal quality factor obtained from our laboratory data agreed very well with the analytical solution. Hence, we concluded that the observed signature frequency (approximately 0.1 MHz) in the seismic coda was indeed a resonance effect. Finally, we have developed possible applications on the reservoir scale to infer fracture-related properties based on seismic coda analysis.

INTRODUCTION

Fractures in rocks contribute to the permeability of a reservoir (Faoro et al., 2009) and could have a significant influence on the seismic signature of the reflected and transmitted waves on a seismic section. For example, the presence of fractures leads to a general reduction of seismic propagation velocity (Peacock et al., 1994; Saenger and Shapiro, 2002), to seismic reflections and diffractions (Groenenboom and Falk, 2000; Ionov, 2007), or to seismic anisotropy (Sayers and Kachanov, 1995; Maultzsch et al., 2003; Zhong et al., 2014). In addition, the presence of fluids in rocks also modifies the properties of a reservoir, leading to dispersion and frequency-dependent attenuation (Biot, 1962; White, 1975; Bourbie et al., 1987; Carcione, 2001; Quintal et al., 2011). Research on understanding these seismic effects in fluid-filled reservoir rocks is essential for various applications of, for example, CO_2 sequestration, hydrocarbon exploration, or underground nuclear waste disposal.

The Krauklis wave is a unique-guided seismic-wave mode that is bound to and propagates along fluid-filled fractures (Krauklis, 1962). It is highly dispersive with a low-phase velocity at low frequencies in a system of a fluid layer (fracture) bounded by two elastic half-spaces (Ferrazzini and Aki, 1987; Chouet, 1996; Ashour, 2000; Korneev, 2008, 2010; Korneev et al., 2009). Because it primarily propagates within the fluid channel formed by a fracture, the related seismic signals can be used for fracture characterization. When a Krauklis wave is trapped and is propagating inside fluid-filled fractures, it is expected to resonate in the fracture, and hence emit seismic signals with a signature frequency. The resonant behavior should prompt strong frequency dependence for seismic body waves, which should in principle permit the identification of Krauklis wave-related signals in the coda of recorded seismograms (Korneev, 2008). Frehner et al. (2009) and Steeb et al. (2010, 2012) study the effect of rock-internal oscillations and find that these oscillations strongly modify the seismic-wave propagation behavior, in particular for seismic waves with

Manuscript received by the Editor 2 February 2016; revised manuscript received 15 June 2016; published online 7 September 2016.
[1]ETH Zurich, Department of Earth Sciences, Zurich, Switzerland. E-mail: pei-ju.shih@erdw.ethz.ch; marcel.frehner@erdw.ethz.ch.

frequencies close to the resonance frequency. A resonant behavior in fluid-filled fractures is widely observed in natural systems, such as glaciers, volcanoes, or geothermal reservoirs. However, Krauklis waves are particularly interesting for hydrofracturing and microseismicity applications. When the fluid is overpressured (hydrofracturing: Ferrazzini et al., 1990), fractures may open corresponding to a seismic source inside the fracture, which easily initiate Krauklis waves (Frehner et al., 2010). Hence, Krauklis waves can be significantly useful for monitoring hydrofracturing operations (Ferrazzini et al., 1990; Groenenbooom and Falk, 2000; Groenenboom and van Dam, 2000). Lipovsky and Dunham (2015) develop analytical relationships between the fracture geometry (thickness and length) and the seismically observed resonance frequency and temporal quality factor.

Aki et al. (1977) and Chouet (1988, 1996) use resonance behavior to show the potential of volcanic eruption forecasting by recording long-period volcanic tremor signals. They assume that the tremor with quasi-constant frequency is generated by fluid resonance in fractures and magma conduits, which therefore provide information of the state of fluid in the subsurface. Tary and Van der Baan (2012) expect Krauklis waves to be the main cause of the observed resonances during fluid injection operations in an oil and gas reservoir, and Tary et al. (2014) relate the observed resonances during hydraulic fracturing activities to Krauklis waves. They demonstrate that the recorded seismic frequency content provides useful information for understanding the geologic reservoir formation. Recently, Nakagawa et al. (2014) observe Krauklis wave-related effects that result in low velocity and large attenuation of the waves while performing laboratory experiments on an analog fracture at a source frequency less than 1 kHz. Krauklis wave-related effects seem to be quite prevalent in several studies and their characteristics might be one of the keys to reveal properties of fluid-bearing fractured rocks.

Current poroelastic theories such as the Biot (1962) model and squirt-flow model (Mavko and Jizba, 1991; Dvorkin et al., 1995) still cannot fully explain the effects of fractures in porous rocks. Korneev et al. (2009) suggest that Krauklis waves might be an important phenomenon to understand the "observed frequency dependent and nonlinear behavior of fluid reservoirs." Several theoretical studies have analytically derived the dispersion behavior of Krauklis waves in infinitely long and straight fractures (Ferrazzini and Aki, 1987; Ashour, 2000; Korneev, 2008, 2010, 2011). Frehner and Schmalholz (2010) state that the resonance behavior of Krauklis waves in fractures should be considered and incorporated into existing effective medium theories to obtain a more representative model for fractured rocks. However, purely analytical methods cannot handle realistic fracture geometries or finite-length fractures. Therefore, we conduct laboratory experiments to visualize fracture-related effects on seismic waves propagating through real fractured materials.

The Krauklis wave cannot be detected at a relatively short distance away from the fracture because of the exponential decay of its amplitude in space. However, Frehner and Schmalholz (2010) demonstrate that Krauklis wave-related signals could be detected as converted body waves as a result of scattering at the crack tips and at irregularities of the fracture. The study also shows that the scattering behavior of Krauklis waves depends significantly on the geometry of the crack tip and on the type of fluid in the crack. Moreover, Frehner (2014) uses a 2D finite-element model to demonstrate that the P- and S-waves are capable of initiating Krauklis waves. The fracture-internal oscillatory behavior of Krauklis waves can be converted to body waves and transmitted into the surrounding rock, which allows a detection away from the fractured reservoir at a seismic receiver.

The initiation of Krauklis waves by body waves strongly depends on the incidence angle and incident wave mode (P- or S-wave). Frehner (2014) shows that incident S-waves initiate larger amplitude Krauklis waves than P-waves. As a result, S-waves may carry more information about fractures, such as fracture orientation or fluid content. The following laboratory study focuses mainly on the case of an incident S-wave. The numerical setup of Frehner (2014) provides the guidelines for our laboratory investigation.

LABORATORY METHODS

We use the ultrasonic pulse transmission method (Birch, 1960; source at position 1, receiver at position 2 in Figure 1a). The fundamental elements of this method are P- or S-wave transducers at either end of the sample, a pulse generator connected with the source transducer, a digital oscilloscope connected with the receiver transducer, and data acquisition software (Figure 1c). The transducers are made of piezoelectric crystals, which convert the electrical signal into acoustic pulses at one end of the sample and vice versa at the other end. The seismic source signal has a dominant frequency of 0.6, 1, and 2.25 MHz. Figure 1c illustrates the experimental setup for P- and S-wave acquisitions. We screw the P-wave transducers into the Plexiglas sample. We then hang the P-wave sample on the top of two light cotton wires to achieve the smallest contact surface between the sample and the means of suspension, minimizing any possible contact effects. The P- and S-wave transducers have different configurations. The S-wave transducers are larger, and therefore cannot be screwed into the sample. We press the transducers against the sample ends. We then place the S-wave sample and transducers between custom-made pressers with a metal weight to enhance the contact between sample and transducers. Specialized coupling gel further enhances the coupling.

We chose a cylindrical Plexiglas sample (120 mm length and 25 mm diameter) containing a single fracture (Figure 1a) as the ideal material to mimic the simplified numerical setup of Frehner (2014). The sample has to be sufficiently long for identifying different P- or S-wave arrivals in the recorded seismograms. At the same time, the sample cannot be too long to avoid losing too much of the source frequency content due to the relatively high-intrinsic attenuation of Plexiglas. We manufactured a 0.1 mm thick fracture by cutting the sample at a given angle, milling on one side a 0.1 mm deep, 25×15 mm elliptical hole, and fusing the two pieces back together with chloroform (Figure 1a and 1b). Chemically fusing the Plexiglas with chloroform results in an isolated fracture, ideally without interfaces around the fracture. Following this procedure, we created samples with fractures at 30°, 45°, and 60° inclination angles. The fracture is filled with air as fluid. Figure 1b shows the segmented micro-CT scan of a sample containing the manufactured fracture, which we used for P-wave experiments. The manufactured fractures (Figure 1b: blue area) for the P- and S-wave experiments are nearly identical.

RESULTS

In the laboratory experiments, we primarily focus on S-wave experiments because numerical simulation results (Frehner, 2014) predict that S-wave initiate Krauklis waves much more efficiently

than P-waves. Therefore, we expect that the recorded seismograms in the S-wave experiments carry more information about the fracture properties. However, we first present few experimental results obtained with the P-wave acquisition setup before we focus on the S-wave results. For the same reason, only the case of 45° fracture orientation has been investigated for P-wave, whereas all three scenarios, i.e., 30°, 45°, and 60° fracture orientations have been investigated for the S-wave.

P-wave experiments

Figure 2 shows the receiver spectra for experiments with a dominant P-wave source frequency of 0.6 and 1 MHz, respectively, for the intact sample and fractured samples with a fracture inclination angle of 45° (traces are provided as supplementary figures that can be accessed through the following links: s1.pdf and s2.pdf). For a source frequency of 0.6 MHz (Figure 2a), the peak amplitude of the signal acquired in the intact sample is 27 μV and occurs at 0.6 MHz; for the fractured sample, amplitude peaks at 0.7 MHz with a maximum value of 13 μV. For a source frequency of 1 MHz (Figure 2b), the frequency peak is at 0.7 MHz with an amplitude of 13 μV for the intact sample and at 0.8 MHz with an amplitude of 7 μV for the fractured sample. Furthermore, the frequency peaks for intact (0.7 MHz) and fractured samples (0.8 MHz) are not exactly at the source frequency (1 MHz) due to the intrinsic attenuation of Plexiglas. For both source frequencies, the peak amplitude for the

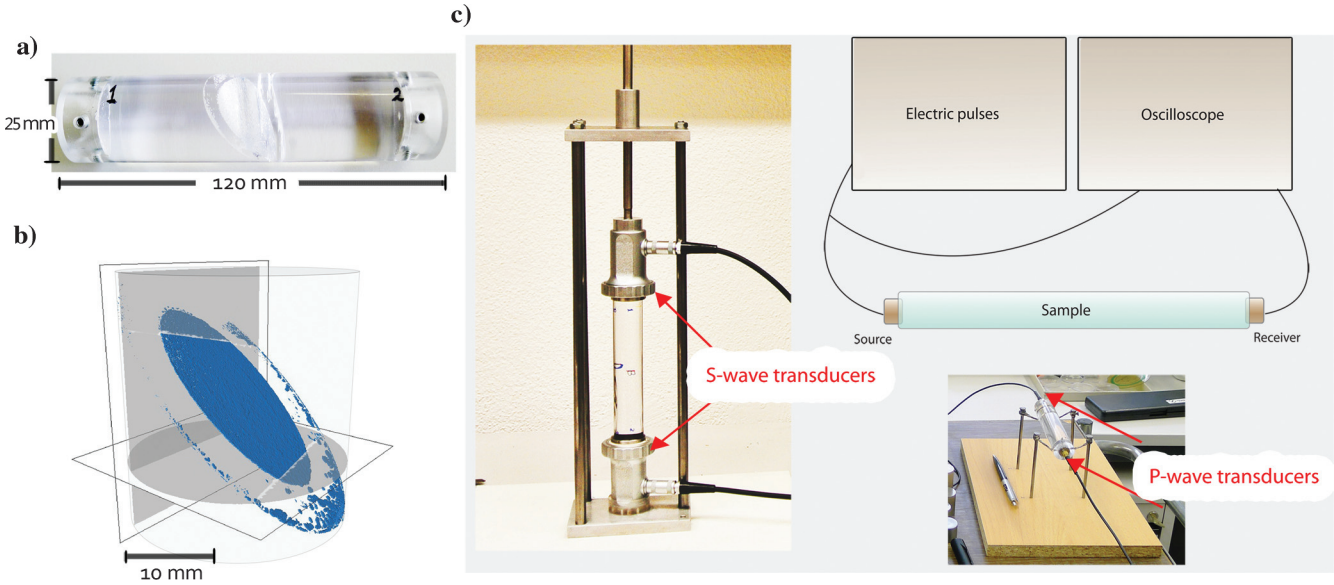

Figure 1. (a) Plexiglas sample (120 mm length and 25 mm diameter) with manufactured elliptical fracture (25 × 15 mm, 0.1 mm thickness, and 45° inclination angle) for P-wave acquisition. (b) Segmented micro-CT scan of the same sample (transparent gray) containing the manufactured fracture (blue). (c) S-wave acquisition setup. The sample is placed between the S-wave transducers under a custom-made presser with a metal weight, which enhances the coupling between the sample and the transducers. One transducer is connected to the electric pulse generator (source), and the other is connected to the oscilloscope (receiver). Inset: P-wave acquisition setup. The sample is hung on the top of two cotton wires to obtain the smallest possible contact surface between the sample and the means of suspension, minimizing any possible contact effects. The P-wave transducers are screwed into the Plexiglas sample.

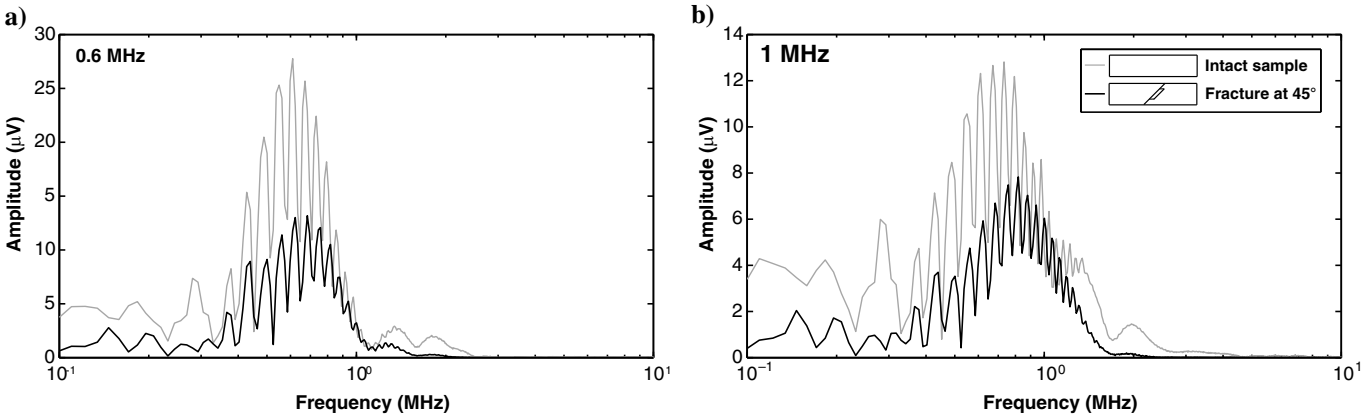

Figure 2. Receiver spectra for experiments with a dominant P-wave source frequency of (a) 0.6 and (b) 1 MHz for the intact sample and fractured samples with a fracture inclination angle of 45°.

fractured sample is about half the magnitude observed for the intact sample, which indicates increased attenuation if the fracture is present. However, the shape of the spectra for the intact and the fractured sample looks similar, indicating that the increased attenuation is almost frequency independent. The slight frequency shift of the peak amplitude is minor and probably not detectable in the case of more realistic rough fracture surfaces, multiple fracture or fracture networks, or added background noise. Therefore, in the case of an incident P-wave, we cannot infer any fracture properties from the acquired data and its spectrum.

S-wave experiments

Figure 3 displays the receiver spectra for an S-wave source with 0.6, 1, and 2.25 MHz dominant source frequency, respectively, for the intact sample and for fractured samples with 30°, 45°, and 60° inclination angles. The source frequency spectra are obtained from signals measured in a steel sample (49.08 mm length) at 0.6, 1, and 2.25 MHz, and are presented in gray in Figure 3. Due to our laboratory setup with piezoelectric transducers, the main energy band of the source is always around the central frequency (1 MHz) of the transducer. For a source frequency of 0.6, 1, and 2.25 MHz (Figure 3a–3c), the amplitude peaks at approximately 0.08 MHz for the intact sample but at approximately 0.04 MHz for the three fractured samples. In addition, the peak amplitudes are reduced compared with the intact sample. The spectra for an inclination angle of 30° and 60° follow the same pattern, whereas the spectrum for a fracture with 45° inclination angle generally exhibits lower amplitudes.

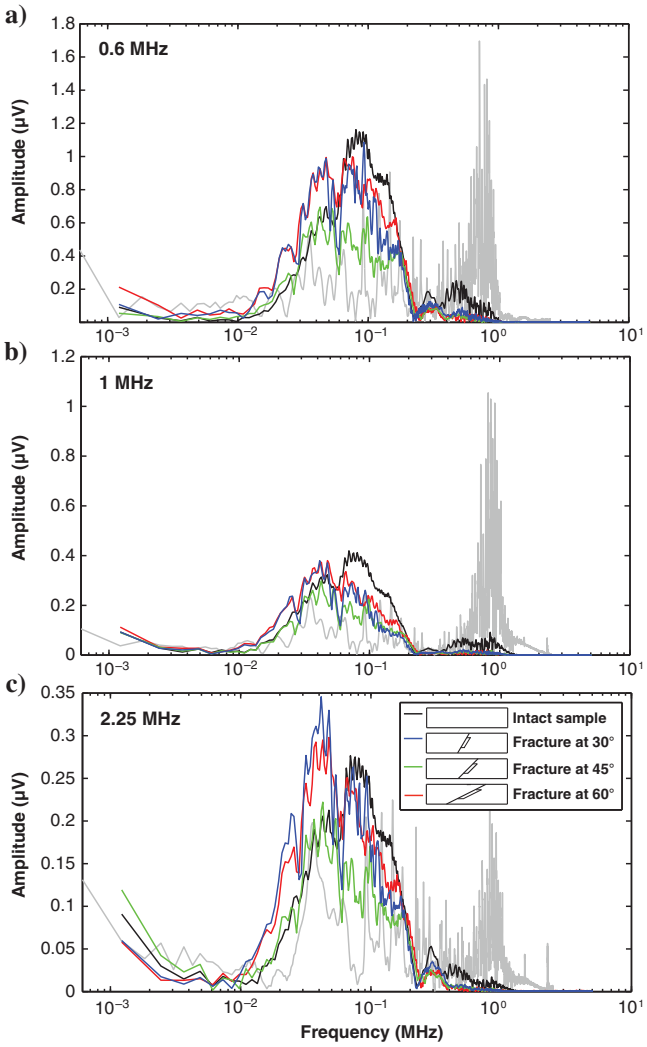

Figure 3. Receiver spectra of the whole trace for experiments with a dominant S-wave source frequency of (a) 0.6, (b) 1, and (c) 2.25 MHz for the intact sample and fractured samples with a fracture inclination angle of 30°, 45°, and 60°, respectively. The source frequency spectra (gray) are obtained from measurements in a steel sample (49.08 mm length).

Despite some differences, the general pattern of the receiver spectra is similar for all fractured experiments at a given source frequency, but significantly different than the spectra for the intact sample. For all three source frequencies, the shape of the spectra for fractured samples with 30° and 60° inclination angles is even almost identical. A fracture-related attenuation can be identified at approximately 0.1 MHz for all three inclination angles. In addition, the receiver spectra for the case of 45° fracture inclination reveal the largest attenuation compared with the cases of 30° and 60° (Figure 3). The frequency of maximum attenuation is independent of the source frequency and fracture orientation, and therefore an intrinsic property of the fracture geometry. These observations give us confidence that there is fracture-related information in the receiver data of S-wave experiments.

The receiver spectra are similar for all source frequencies because of the piezoelectric transducers (Figure 3). As an exemplary case, we focus on results for the dominant source frequency of 1 MHz for further detailed interpretation (Figures 4 and 5) because the seismic effects are best visible at this source frequency. The receiver spectra for the 30°, 45°, and 60° fracture inclination angles (Figure 3b) indicate strong attenuation at 0.1 MHz; hence, the time signals are converted to spectrograms for further investigation. Figure 4 presents the spectrograms of the normalized receiver data for different fracture inclination angles (30°, 45°, and 60°) and for the intact sample. The receiver time signal is normalized by dividing its maximum amplitude before converting it to a spectrogram. After 50 μs, the P-wave first arrival can be identified and after approximately 100 μs the S-wave first arrival follows. The dominant frequency of the P-wave is approximately 1 MHz, but the intensity decreases for the fractured samples (Figure 4b–4d). The dominant frequency of the S-wave arrival is approximately 0.6 and 0.2 MHz for the intact and fractured samples, respectively. However, at 0.6 MHz, the intensity decreases for the fractured samples (Figure 4b–4d), but remains similar at 0.2 MHz. Moreover, after approximately 300 μs, a multiple S-wave reflection can be identified in the intact sample (Figure 4a).

The vertical white dashed line (150 μs) separates the first arrivals (direct P- and S-waves) and the subsequent coda, whereas the latter is the primary focus here. The presence of the fracture induces elevated amplitudes at low frequencies in the coda after the first arrival (150 μs onward, Figure 4b–4d). This fracture-related effect is very narrow banded exhibiting a signature frequency at approximately 0.1 MHz and decays relatively slowly over time. The observed signature frequency is independent of the fracture orientation and used source frequency. Note that the coda for the 45° fracture inclination (Figure 4c) exhibits relatively larger amplitude approximately 0.1 MHz compared with the cases of 30° and 60°.

Because the presence of the fracture leads to elevated amplitudes at low frequencies in the coda (Figure 4b–4d), we now focus on

frequencies less than 0.1 MHz. Figure 5 displays the low-pass filtered receiver time signal representing a frequency band of 0–0.1 MHz. For low-pass filtering, we used a fourth-order Butterworth filter with a cut-off frequency of 0.1 MHz. Within this frequency band, we assume an exponential amplitude decay of the coda over time (i.e., linear decay in the logarithmic plot, Figure 5). Hence, we calculate the decay coefficients using a linear fit (in logarithmic representation) through the first S-wave arrival peak and local maximum peaks of the filtered time signal up to 250 μs. We chose the upper time limit because multiple reflections occur at approximately 300 μs (Figure 4). For the linear fit, we only selected local maximum peaks that are significantly larger than the background signal level. This background level can be inferred from the signal prior to the first P-wave arrival as −4 mV (Figure 5); hence, we only used local maxima with an amplitude greater than −3.75 mV.

The resulting decay coefficients based on the $\log_{10}$ data representation (i.e., slope of linear fit in Figure 5) are given in Figure 5 and listed in Table 1 together with the recalculated values for a $\log_e$ data representation. The decay coefficient represents the decay of the coda signal over time. For the fractured samples (Figure 5b–5d), the coda amplitudes decay relatively slowly over time compared with the intact sample, which demonstrates the fracture-related effects (Figure 5). The decay coefficients (in $\log_{10}$ representation) for the fractured samples are lower than for the intact sample (Figure 5; Table 1).

To clearly define temporal quality factor Q_{temporal}, we consider at the exponentially decaying values of the amplitude-versus-time signal $A(t)$ (section 5.5; Aki and Richards, 2002)

$$A(t) = A_0 \exp(-\alpha t), \tag{1a}$$

$$\alpha = \frac{\pi f_r}{Q_{\text{temporal}}}. \tag{1b}$$

The temporal quality factor Q_{temporal} (i.e., inverse measure for temporal decay) can be obtained from the temporal decay coefficient α (in $\log_e$ data representation; Table 1) and the observed characteristic resonant frequency f_r.

The temporal quality factor Q_{temporal} for the fractured samples is similar for the different fracture inclination angles and distinctively different from the intact sample (Table 1). This indicates that the relatively large temporal quality factor is due to the presence of the fracture but independent of fracture orientation. In general, low Q_{temporal} values indicate large dissipation. On first sight, the low Q_{temporal} value for the intact sample might seem contradictory because we expect stronger attenuation in the fractured samples. However, the temporal quality factor calculated here does not represent attenuation of a propagating wave (the spatial quality factor would do that), but the decay of the coda signal over time. Here, the coda is generated by a resonance effect in the fracture; hence, the temporal quality factor represents the damping of an oscillatory movement. In the intact sample, this resonance effect does not occur; hence, the coda is almost inexistent and decays rapidly (i.e., low Q_{temporal} value).

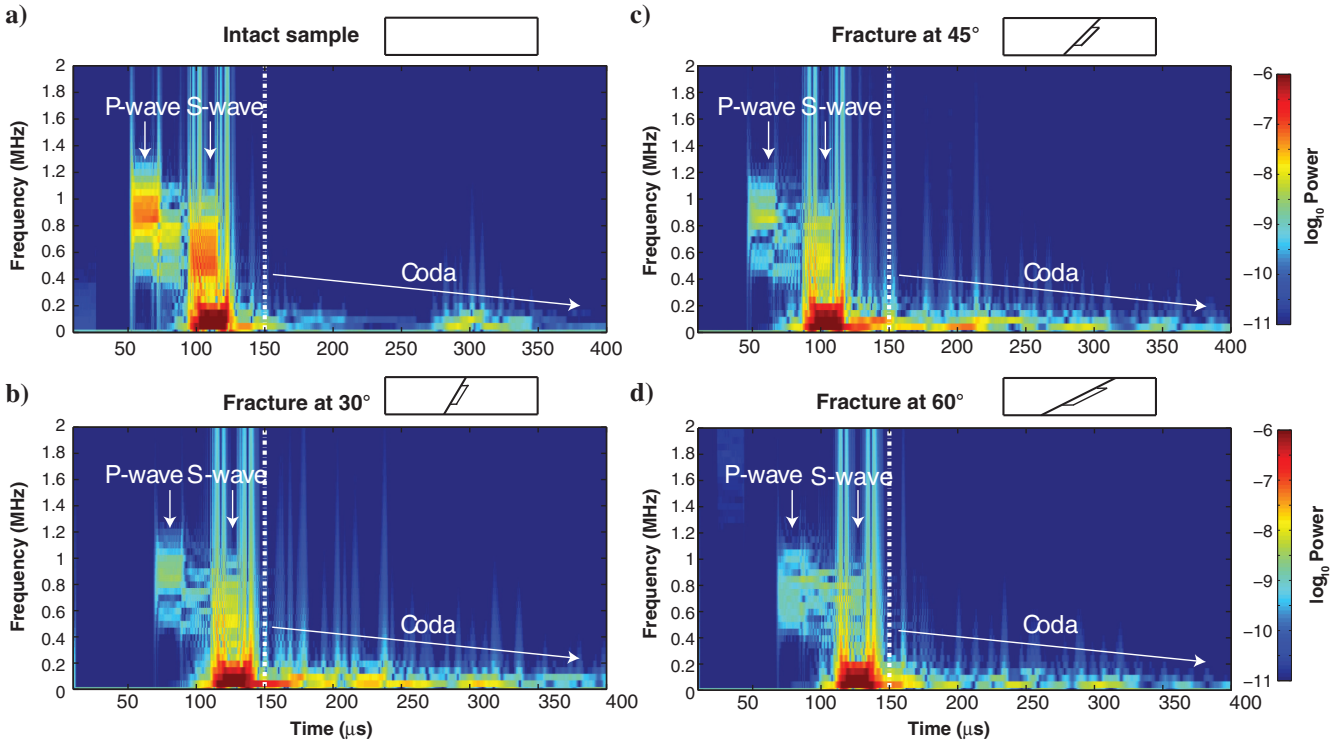

Figure 4. (a) Spectrograms of normalized receiver time signals generated by an S-wave with a dominant source frequency of 1 MHz propagating through the intact sample, and through fractured samples with a fracture inclination angle of (b) 30°, (c) 45°, and (d) 60°, respectively. The color bar represents power spectral density. The vertical dashed line (150 μs) separates the first arrivals (direct P- and S-waves) and the subsequent coda.

Analytical solution

It is critical to realize that the temporal quality factor Q_{temporal} permits the observation of temporal signal decay at a specific point; it should not be confused with the more commonly used spatial quality factor that describes the spatial decay of a propagating wave. Lipovsky and Dunham (2015) develop analytical solutions relating the aperture (i.e., fracture width) and length of a fracture to the seismically observed characteristic resonance frequency f_r and temporal quality factor Q_{temporal}

$$L = \frac{1}{2}\left[\pi\nu\left(\frac{G_s}{(1-v_s)\rho}\right)^2 \frac{Q_{\text{temporal}}^2}{f_r^5}\right]^{1/6}, \quad (2)$$

$$2w = Q_{\text{temporal}}\sqrt{\nu/(\pi f_r)}, \quad (3)$$

where, for our case, L is the fracture length, ν is the kinematic viscosity of air, G_s is the shear modulus of Plexiglas, v_S is the Poisson's ratio of Plexiglas, ρ is the density of air, and w is the fracture half-width. The two factors leading to an exponential amplitude decay of the oscillatory signal in the coda are fluid viscosity and emitted seismic energy (Aki, 1984; Chouet, 1992). Decay in the model of Lipovsky and Dunham (2015) is due to fluid viscosity alone. Using these equations, the observed characteristic resonant frequency f_r and quality factor Q_{temporal} uniquely constrain the fracture geometry, if the fluid and solid mechanical properties are known. Here, we use the equations to calculate Q_{temporal} from the known mechanical and geometric parameters used in our laboratory experiment. Table 2 displays the input data for our laboratory case.

The temporal quality factor we obtain from equation 2 ($Q_{\text{temporal}} = 23.2$) is very close to the value derived from our laboratory data ($19.8 < Q_{\text{temporal}} < 21.4$; Table 1); the value we obtain

Table 1. Decay coefficients obtained from $\log_{10}$ data representation (Figure 5), recalculated decay coefficients in $\log_e$ representation (input for equation 1), and temporal quality factor (output from equation 1).

Sample	Decay coefficient in $\log_{10}$ representation $\alpha/\log_e(10)$ (μs^{-1}) (see Figure 5)	Decay coefficient in $\log_e$ representation α (μs^{-1}) (for equation 1)	Temporal quality factor Q_{temporal} (−) (from equation 1)
Intact sample	2.2×10^{-2}	5.1×10^{-2}	6.2
Fracture at 30°	6.5×10^{-3}	15.0×10^{-3}	20.9
Fracture at 45°	6.4×10^{-3}	14.7×10^{-3}	21.4
Fracture at 60°	6.9×10^{-3}	15.9×10^{-3}	19.8

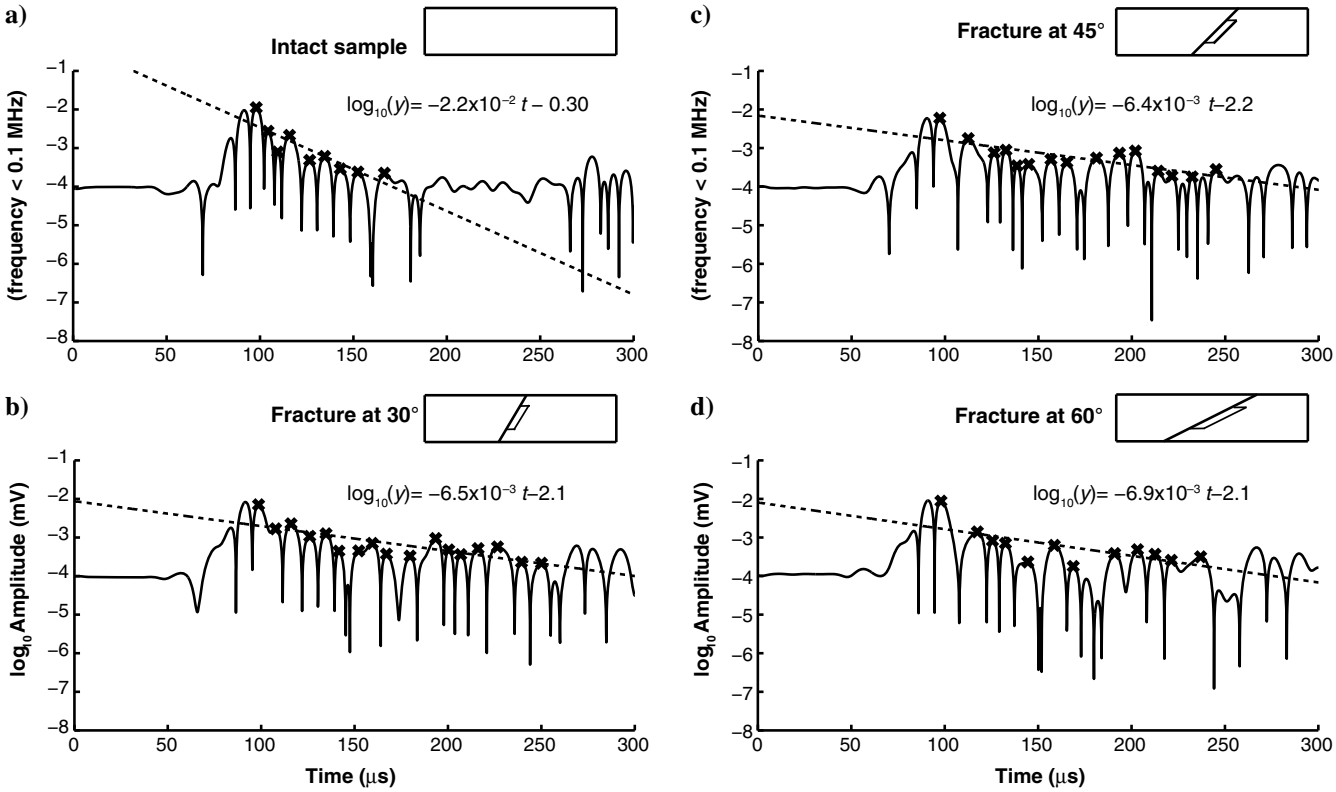

Figure 5. Low-pass filtered receiver time signal with a frequency band of 0–0.1 MHz, representing the coda generated by an S-wave with a dominant source frequency of 1 MHz propagating through (a) the intact sample, and through fractured samples with a fracture inclination angle of (b) 30°, (c) 45°, and (d) 60°, respectively. A fourth-order Butterworth filter with a cut-off frequency of 0.1 MHz was used for low-pass filtering the receiver time signal.

from equation 3 ($Q_{\text{temporal}} = 14.0$) is slightly too low but still in the right order of magnitude. However, equation 3 is based on the fracture aperture w (i.e., thickness) that is much less precise during fracture manufacturing than the length L used in equation 2. For example, already for a slightly thicker fracture with $w = 0.071$ mm, the temporal quality factor increases to $Q_{\text{temporal}} = 20.0$. In any case, we use the very good match between the analytically derived (Table 2) and the laboratory data derived (Table 1) temporal quality factor as an indicator for the validity of our assumption that the observed signature frequency in the coda (approximately 0.1 MHz) is indeed caused by resonance effects due to Krauklis waves in the fracture.

DISCUSSION

In our experiments, the presence of a fracture leads to a spectral peak at a signature frequency of approximately 0.1 MHz (Figures 3 and 4). This fracture-related peak is very narrow banded, decays slowly after the arrival of the direct wave, and its decay coefficient (i.e., temporal quality factor) is independent of the fracture orientation (Figure 5; Table 1); the signature frequency itself is also independent of the fracture orientation (Figure 4). Therefore, we interpret this enhanced amplitude to be due to oscillation effects (i.e., resonance) related to Krauklis waves in the fracture. In addition, the resonance frequency is an intrinsic property of the fracture geometry and elastic properties, and it is independent of the dominant source frequency. In addition, the close agreement between the analytically derived and the laboratory derived temporal quality factor supports our interpretation, as the analytical solution (Lipovsky and Dunham, 2015) is based on Krauklis-wave resonance.

Frehner et al. (2009, 2010) and Steeb et al. (2012) develop theoretical models with increasing complexity for seismic waves propagating through media exhibiting medium-internal oscillations. The argument for oscillations are different in these publications, but the models may well be applied to Krauklis-wave oscillation in fractures. All these studies calculate the velocity dispersion and attenuation relations demonstrating a strong frequency-dependent propagation behavior for body waves. In addition, Frehner et al. (2009) develop a dynamic finite-difference model to simulate propagating waves, record seismograms, and calculate a receiver spectrogram (their Figure 5). The spectrogram shows that the incident body wave loses energy triggering the oscillatory system at the resonance frequency. However, after the first arrival of the body wave, the system continues to oscillate with its resonance frequency leading to a very narrow-banded coda that decays exponentially over time. The obvious similarities to our laboratory study further strengthen our interpretation that the observed coda is a result of medium-internal oscillations, in our case resonating Krauklis waves in the fracture.

Figure 4 indicates that the narrow-banded coda signal has a slightly larger amplitude for a fracture inclination of 45° compared with 30° and 60°. This agrees with the numerical study of Frehner (2014), which demonstrates that Krauklis waves initiated by an incident S-wave have the largest amplitude for a fracture inclination of approximately 50° and decreasing amplitudes for smaller and larger inclinations. For larger Krauklis-wave amplitudes, we also expect larger amplitude oscillations in the fracture and ultimately a larger amplitude coda signal. In our laboratory study, we do not consider the amplitude difference between the different inclination angles to be sufficient to infer the fracture orientations from the narrow-banded coda signal. However, in principle it should be possible to infer fracture orientations from coda analysis. In addition, Frehner and Schmalholz (2010) demonstrate that body waves emitted from a fracture due to Krauklis-wave scattering exhibit particular P- and S-wave radiation patterns. Therefore, not only the absolute coda amplitude at one single receiver but also the spatial distribution of coda signals and their P- and S-wave contents, as measured by multiple receivers, might help decipher fracture orientation.

Scattering effect

To verify whether scattering effects could contribute to the observed coda signal at 0.1 MHz, we estimate the frequency of dominant scattering in our laboratory setting. Frehner and Schmalholz (2010) and Frehner (2014) present high-resolution numerical models of seismic wave scattering at fractures and show that the main source of scattering is the fracture tips. Therefore, we can assume that the fracture width, and not the fracture length, is the controlling length scale for scattering. Given the S-wave velocity for Plexiglas of 1200 m/s (i.e., wavelength of 12 mm at 0.1 MHz), the ratio between wavelength and scatterer size is 120. This ratio is well above the Rayleigh scattering limit (section 3.14, Mavko et al., 2009). Therefore, we can assume that scattering does not play a significant role at the observed 0.1 MHz coda signal.

Limitations

Figure 3 shows that only small amplitudes at the dominant source frequencies arrive at the receiver due to the relatively large intrinsic attenuation of Plexiglas. Therefore, we repeated the measurements with reduced sample lengths (<60 mm, i.e., less than half of our standard samples) and observed larger amplitudes at the source frequency. This implies that the intrinsic attenuation of Plexiglas is causing significant attenuation at the source frequency. For the shorter sample lengths, the low-frequency spectral shapes up to 0.2 MHz are similar to those of 120 mm sample length but with slightly higher absolute magnitudes. Regardless of the attenuation at the source frequency, we chose the longer samples (120 mm) for a clear separation between the direct P- and S-wave arrivals and between the coda and the first body wave reflections.

The major differences between our laboratory setup and the numerical setup of Frehner (2014) are the source and receiver positions, the filling of the fracture, and the source frequency range. The numerical simulations were done in 2D, and a virtual receiver

Table 2. Input parameters for equations 2 and 3 and the resulting temporal quality factor Q_{temporal}.

Equation 2		Equation 3	
L	25×10^{-3} m	w	5×10^{-5} m
ν	1.6×10^{-5} m^2/s	ν	1.6×10^{-5} m^2/s
G_s	1.71 GPa	f_r	0.1 MHz
P	1.184 kg/m^3	—	—
v_s	0.4	—	—
f_r	0.1 MHz	—	—
Q_{temporal}	23.2	Q_{temporal}	14.0

line is placed parallel to and inside the fracture; in the laboratory experiments, we placed the source and receiver transducers on both ends of the sample. In the numerical simulations, the fracture is filled with water; in the laboratory, the fracture is filled with air. The dominant source frequency in the numerical simulations is in kilohertz, whereas it is in megahertz in the laboratory experiments. Due to these differences, our laboratory results may not be directly comparable with the numerical simulations of Frehner (2014). In particular, the numerical receiver positions are impossible to translate to the laboratory setup; hence, the receiver signals are not comparable. Despite these different setups, our laboratory results coincide with the numerical results (Frehner, 2014), in that, we confirm the largest effect of the fracture in the case of an incident S-wave and at a fracture inclination angle of 45°.

Implications and possible applications

We demonstrated that the presence of a fracture causes seismic coda exhibiting a signature frequency. This narrow-banded coda is caused by Krauklis-wave resonance in the fracture, which decays exponentially over time. Based on our observations and interpretations, we propose that seismic coda analysis, in particular in the frequency-time domain, provides useful information about the fracture system. As demonstrated by Lipovsky and Dunham (2015), the signature frequency together with the temporal quality factor constrains the fracture geometry, if the mechanical properties of the rock and fluid are known. In addition, we propose that the analysis of absolute coda amplitudes at a single station and/or the comparison of coda signals at multiple stations provides information about the fracture orientation. In a naturally fractured reservoir, fractures have different sizes and crosscut each other. Compared with our laboratory study on one simplified single fracture, in natural systems, we expect less narrow-banded coda signals (due to different fracture sizes) and more difficult to interpret absolute coda amplitudes and temporal quality factors (due to multiple fracture orientations).

A possible future application in field-scale settings may be time-lapse seismic coda analysis to monitor fracture development during hydrofracturing operations. In addition to standard seismic monitoring techniques (e.g., microseismicity triangulation based on first arrivals), an increase of coda amplitude can indicate fracture density or coda analysis on seismic arrays may help to constrain the dominant fracture orientations. Hydrofracturing operations are particularly suited for Krauklis wave-related studies because the seismic sources are located within the fracture system, which results in large Krauklis-wave amplitudes. Of course, this also applies for nonman-made hydrofracturing situations, such as overpressured magmatic or hydrothermal systems, which also require monitoring.

A second possible application may be coda analysis in active seismic surveys. In this case, the seismic source is outside the fracture system, similar to our laboratory experiments. For an enhanced triggering of Krauklis-wave resonance, we recommend using a seismic source that radiates S-waves. Coda analysis in active seismic surveys may allow inferring fracture density and orientation. The exponential decay of the coda amplitude with time may be used to infer fluid viscosity within a fracture system; hence, coda analysis may help to locate the oil/water and oil/gas contact in a hydrocarbon reservoir. In boreholes, seismic coda analysis may be used to infer fracture damage in the surrounding rock volume.

CONCLUSION

In our laboratory study, we recorded receiver signals from propagating ultrasonic waves through a Plexiglas sample without a fracture and samples with a single well-defined fracture with different inclination angles of 30°, 45°, and 60°. The experimental results of an incident P-wave showed that the presence of a fracture has a negligible effect, which does not allow inferring fracture-related properties. In contrast, the experimental results of an incident S-wave confirm that the presence of a fracture leads to resonance effects with a signature frequency, which slowly decay over time in the recorded seismic coda. The signature frequency is an intrinsic property of the fracture geometry and the elastic parameters of the sample and fracture, independent of fracture orientation and dominant source frequency. We interpret this resonance to be caused by Krauklis waves initiated by the incident S-wave, and thereafter propagating back and forth in the fracture. The temporal quality factors obtained from our laboratory study agree very well with a published analytical solution, confirming the validity of our interpretation. The 45° fracture inclination results in relatively larger resonance amplitude compared with the 30° or 60° cases. Based on our observations and interpretations, we conclude that seismic coda analysis can deliver useful fracture-related information, such as fracture geometry (length and width), fracture orientation, or fluid viscosity within fractures.

ACKNOWLEDGMENTS

We acknowledge support by the Swiss National Science Foundation (project UPseis, 143319). We thank N. Tisato for constant inputs and helpful discussions. We thank R. Hofmann for his efficient technical support.

REFERENCES

Aki, K., 1984, Evidence for magma intrusion during the mammoth lakes earthquakes of May 1980 and implications of the absence of volcanic (harmonic) tremor: Journal of Geophysical Research, **89**, 7689–7696, doi: 10.1029/JB089iB09p07689.

Aki, K., M. Fehler, and S. Das, 1977, Source mechanism of volcanic tremor: Fluid-driven crack models and their application to the 1963 Kilauea eruption: Journal of Volcanology and Geothermal Research, **2**, 259–287, doi: 10.1016/0377-0273(77)90003-8.

Aki, K., and P. G. Richards, 2002, Quantitative seismology: University Science Books.

Ashour, A. S., 2000, Wave motion in a viscous fluid-filled fracture: International Journal of Engineering Science, **38**, 505–515, doi: 10.1016/S0020-7225(99)00045-2.

Biot, M. A., 1962, Mechanics of deformation and acoustic propagation in porous media: Journal of Applied Physics, **33**, 1482–1498, doi: 10.1063/1.1728759.

Birch, F., 1960, The velocity of compressional waves in rocks to 10 kilobars, Part 1: Journal of Geophysical Research, **65**, 1083–1102, doi: 10.1029/JZ065i004p01083.

Bourbie, T., O. Coussy, and B. Zinszner, 1987, Acoustics of porous media: Editions Technip.

Carcione, J. M., 2001, Wave fields in real media: Wave propagation in anisotropic, anelastic and porous media: Pergamon Press.

Chouet, B., 1988, Resonance of a fluid-driven crack: Radiation properties and implications for the source of long-period events and harmonic tremor: Journal of Geophysical Research, **93**, 4375–4400, doi: 10.1029/JB093iB05p04375.

Chouet, B.., 1992, A seismic model for the source of long-period events and harmonic tremor in volcanic seismology, in P. Gasparini, R. Scarpa, and K. Aki, eds., IAVCEI Proceedings in Volcanology: Springer Verlag, 133–156.

Chouet, B., 1996, Long-period volcano seismicity: Its source and use in eruption forecasting: Nature, **380**, 309–316, doi: 10.1038/380309a0.

Dvorkin, J., G. Mavko, and A. Nur, 1995, Squirt flow in fully saturated rocks: Geophysics, **60**, 97–107, doi: 10.1190/1.1443767.

Faoro, I., A. Niemeijer, C. Marone, and D. Elsworth, 2009, Influence of shear and deviatoric stress on the evolution of permeability in fractured rock: Journal of Geophysical Research, **114**, B01201, doi: 10.1029/2007JB005372.

Ferrazzini, V., and K. Aki, 1987, Slow waves trapped in a fluid-filled infinite crack: Implication for volcanic tremor: Journal of Geophysical Research, **92**, 9215–9223, doi: 10.1029/JB092iB09p09215.

Ferrazzini, V., B. Chouet, M. Fehler, and K. Aki, 1990, Quantitative-analysis of long-period events recorded during hydrofracture experiments at Fenton Hill, New Mexico: Journal of Geophysical Research, **95**, 21871–21884, doi: 10.1029/JB095iBl3p21871.

Frehner, M., 2014: Krauklis wave initiation in fluid-filled fractures by seismic body waves: Geophysics, **79**, no. 1, T27–T35, doi: 10.1190/GEO2013-0093.1.

Frehner, M., and S. M. Schmalholz, 2010, Finite-element simulations of Stoneley guided-wave reflection and scattering at the tips of fluid-filled fractures: Geophysics, **75**, no. 2, T23–T36, doi: 10.1190/1.3340361.

Frehner, M., S. M. Schmalholz, and Y. Podladchikov, 2009, Spectral modification of seismic waves propagating through solids exhibiting a resonance frequency: A 1-D coupled wave propagation-oscillation model: Geophysical Journal International, **176**, 589–600, doi: 10.1111/j.1365-246X.2008.04001.x.

Frehner, M., H. Steeb, and S. M. Schmalholz, 2010, Wave velocity dispersion and attenuation in media exhibiting internal oscillations, *in* A. Petrin, ed., Wave propagation in materials for modern applications: In-Tech Education and Publishing, 455–476.

Groenenboom, J., and J. Falk, 2000, Scattering by hydraulic fractures: Finite-difference modeling and laboratory data: Geophysics, **65**, 612–622, doi: 10.1190/1.1444757.

Groenenboom, J., and D. B. van Dam, 2000, Monitoring hydraulic fractures growth: Laboratory experiments: Geophysics, **65**, 603–611, doi: 10.1190/1.1444756.

Ionov, A. M., 2007, Stoneley wave generation by an incident P-wave propagating in the surrounding formation across a horizontal fluid-filled fracture: Geophysical Prospecting, **55**, 71–82, doi: 10.1111/j.1365-2478.2006.00577.x.

Korneev, V., 2008, Slow waves in fractures filled with viscous fluid: Geophysics, **73**, no. 1, N1–N7, doi: 10.1190/1.2802174.

Korneev, V., 2010, Low-frequency fluid waves in fractures and pipes: Geophysics, **75**, no. 6, N97–N107, doi: 10.1190/1.3484155.

Korneev, V., 2011, Krauklis wave in a stack of alternating fluid-elastic layers: Geophysics, **76**, no. 6, N47–N53, doi: 10.1190/geo2011-0086.1.

Korneev, V. A., A. A. Ponomarenko, and M. Kashtan, 2009, Stoneley guided waves: What is missing in Biot's theory?, *in* H. I. Ling, A. Smyth, and R. Betti, eds., Poromechanics IV: Proceedings of the Fourth Biot Conference on Poromechanics: DEStech Publications Inc., 706–711.

Krauklis, P. V., 1962, About some low frequency oscillations of a liquid layer in elastic medium: Prikladnaya Matematikai Mekhanika, **26**, 1111–1115.

Lipovsky, B. P., and E. M. Dunham, 2015, Vibrational modes of hydraulic fractures: Inference of facture geometry from resonant frequencies and attenuation: Journal of Geophysical Research, **120**, 1080–1107, doi: 10.1002/2014JB011286.

Maultzsch, S., M. Chapman, E. Liu, and X. Y. Li, 2003, Modeling frequency-dependent seismic anisotropy in fluid-saturated rock with aligned fractures: Implication of fracture size estimation from anisotropic measurements: Geophysical Prospecting, **51**, 381–392, doi: 10.1046/j.1365-2478.2003.00386.x.

Mavko, G., and D. Jizba, 1991, Estimating grain-scale fluid effects on velocity dispersion in rocks: Geophysics, **56**, 1940–1949, doi: 10.1190/1.1443005.

Mavko, G., T. Mukerji, and J. Dvorkin, 2009, The rock physics handbook: Tools for seismic analysis of porous media: Cambridge University Press.

Nakagawa, S., S. Nakashima, and V. A. Korneev, 2014, Laboratory measurements of guided-wave propagation within a fluid-saturated fracture: Geophysical Prospecting, **64**, 1–14, doi: 10.1111/1365-2478.12223.

Peacock, S., C. McCann, J. Sothcott, and T. R. Astin, 1994, Experimental measurements of seismic attenuation in microfractured sedimentary rock: Geophysics, **59**, 1342–1351, doi: 10.1190/1.1443693.

Quintal, B., H. Steeb, M. Frehner, and S. M. Schmalholz, 2011, Quasi-static finite element modeling of seismic attenuation and dispersion due to wave-induced fluid flow in poroelastic media: Journal of Geophysical Research, **116**, B01201, doi: 10.1029/2010JB007475.

Saenger, E. H., and S. A. Shapiro, 2002, Effective velocities in fractured media: A numerical study using the rotated staggered finite-difference grid: Geophysical Prospecting, **50**, 183–194, doi: 10.1046/j.1365-2478.2002.00309.x.

Sayers, C. M., and M. Kachanov, 1995, Microcrack-induced elastic wave anisotropy of brittle rocks: Journal of Geophysical Research, **100**, 4149–4156, doi: 10.1029/94JB03134.

Steeb, H., M. Frehner, and S. M. Schmalholz, 2010, Waves in residual saturated porous media, *in* G. A. Maugin, and A. V. Metrikine, eds., Mechanics of generalized continua: One hundred years after the Cosserats: Springer Verlag, 9–190.

Steeb, H., P. Kurzeja, M. Frehner, and S. M. Schmalholz, 2012, Phase velocity dispersion and attenuation of seismic waves due to trapped fluids in residual saturated porous media: Vadose Zone Journal, **11**, doi: 10.2136/vzj2011.0121.

Tary, J. B., and M. Van der Baan, 2012, Potential use of resonance frequencies in microseismic interpretation: The Leading Edge, **31**, 1338–1346, doi: 10.1190/tle31111338.1.

Tary, J. B., M. Van der Baan, and D. W. Eaton, 2014, Interpretation of resonance frequencies recorded during hydraulic fracturing treatments: Journal of Geophysical Research, **119**, 1295–1315, doi: 10.1002/2013JB010904.

White, J. E., 1975, Computed seismic speeds and attenuation in rocks with partial gas saturation: Geophysics, **40**, 224–232, doi: 10.1190/1.1440520.

Zhong, X., M. Frehner, K. Kunze, and A. Zappone, 2014, A novel EBSD-based finite-element wave propagation model for investigating seismic anisotropy: Application to Finero Peridotite, Ivrea-Verbano Zone, Northern Italy: Geophysical Research Letters, **41**, 7105–7114, doi: 10.1002/2014GL060490.